

# Surface origin and control of resonance Raman scattering and surface band gap in indium nitride

Esther Alarcón-Lladó<sup>1,2,4</sup>, Tommaso Brazzini<sup>2,3,5</sup> and Joel W Ager<sup>2</sup>

<sup>1</sup> Swiss Federal Institute of Technology (EPFL), Lausanne, Switzerland

<sup>2</sup> Materials Sciences Division, Lawrence Berkeley National Laboratory, Berkeley, CA, USA

<sup>3</sup> Departamento de Ingeniería Electrónica and Instituto de Sistemas Optoelectrónicos y Microtecnología, ETSI Telecomunicación, Universidad Politécnica de Madrid, 28040 Madrid, Spain

<sup>4</sup> FOM Institute AMOLF, Amsterdam, Netherlands

E-mail: [JWAger@lbl.gov](mailto:JWAger@lbl.gov)

Received 13 November 2015, revised 13 February 2016

Accepted for publication 25 April 2016

Published 23 May 2016



## Abstract

Resonance Raman scattering measurements were performed on indium nitride thin films under conditions where the surface electron concentration was controlled by an electrolyte gate. As the surface condition is tuned from electron depletion to accumulation, the spectral feature at the expected position of the ( $E_1$ ,  $A_1$ ) longitudinal optical (LO) near  $590\text{ cm}^{-1}$  shifts to lower frequency. The shift is reversibly controlled with the applied gate potential, which clearly demonstrates the surface origin of this feature. The result is interpreted within the framework of a Martin double resonance, where the surface functions as a planar defect, allowing the scattering of long wavevector phonons. The allowed wavevector range, and hence the frequency, is modulated by the electron accumulation due to band gap narrowing. A surface band gap reduction of over 500 meV is estimated for the conditions of maximum electron accumulation. Under conditions of electron depletion, the full InN bandgap ( $E_g = 0.65\text{ eV}$ ) is expected at the surface. The drastic change in the surface band gap is expected to influence the transport properties of devices which utilize the surface electron accumulation layer.


Keywords: Raman spectroscopy, indium nitride, surface electron accumulation

(Some figures may appear in colour only in the online journal)

## 1. Introduction

The origin of the intense peak appearing in the resonance Raman spectrum of wurtzite InN films in the vicinity of the expected ( $E_1$ ,  $A_1$ ) longitudinal optical (LO) frequency has been of considerable interest for the last decade. In contrast to GaAs and other III–V semiconductors, where the LO phonon couples to free carriers and forms coupled  $L^-$  and  $L^+$  modes [1], the LO-like scattering in InN and in In-rich InGaN has only a small shift in frequency regardless of electron (hole) concentration [2, 3]. A number of groups have attributed the

LO-like feature observed in the  $z(-,-)z$  scattering geometry from  $c$ -axis oriented wurtzite InN films to an unscreened  $A_1(\text{LO})$  mode with a large wavevector ( $q$ ) [4, 5]. The phonon is uncoupled from the typically large (degenerate) free electron densities due to the breakdown of the  $q$ -conservation. Some authors have attributed the wavevector non-conservation to the presence of bulk impurities [6]. However, this explanation appears to be inconsistent with Cusco *et al* who confirmed the conservation of wavevector in the scattering process in bulk InN by the observation of the  $L^-$  phonon–plasmon coupled mode in a series of doped InN layers [7].

 Original content from this work may be used under the terms of the [Creative Commons Attribution 3.0 licence](https://creativecommons.org/licenses/by/3.0/). Any further distribution of this work must maintain attribution to the author(s) and the title of the work, journal citation and DOI.

<sup>5</sup> Author to whom any correspondence should be addressed.  
Current address: Center for Device Thermography and Reliability (CDTR), H.H. Wills Physics Laboratory, University of Bristol, Tyndall Avenue, Bristol BS8 1TL, United Kingdom.

Recently, a double resonance mechanism was proposed by Davydov *et al* to explain the presence of large- $q$  phonons in the Raman spectra of InN [8]. The mechanism is based on the double resonance theory of Martin [9], and a strong dependence of the frequency of the LO modes on the excitation frequency is predicted and observed. A similarly strong dispersion of the LO-like scattering with excitation frequency was also observed in InN nanowires, providing further support for a double resonance mechanism [10]. However, this proposed scattering mechanism relies on elastic scattering of photoexcited carriers in the intermediate Raman state, which is attributed to the presence of impurities in the bulk material. Also, the LO-like scattering is assumed to have its origin in the bulk of the material.

There is recent evidence that the surface may play an important role in the Raman scattering of InN thin films. For example, Cho *et al* have used cross-sectional Raman microscopy to observe a large increase in scattering from the surface of InN thin films [11]. Kranert *et al* have proposed a model for wurtzite semiconductors in which wave-vector nonconservation can be caused, under resonant excitation conditions, by considering the surface as a planar defect [12].

In this work we critically examine the attribution of the LO-like scattering to the bulk of the InN films. InN is well-known to have a surface electron accumulation (SEA) layer with an areal density in the low-mid  $10^{13} \text{ cm}^{-2}$  range [13], regardless of the surface orientation [14, 15]. The SEA layer, which is depicted schematically in figure 1(a), extends over a range of ca. 10 nm given the range of electron (hole) concentrations observed in bulk of InN films ( $10^{17}$ – $10^{19} \text{ cm}^{-3}$ , typically) [14, 16]. While the presence of the SEA layer has prevented the realization of many traditional semiconductor device architectures, a number of InN-based devices have been demonstrated which utilize the SEA as a conducting channel. These include chemical and anion-sensitive sensors [17, 18] and both electrolyte and dielectric-gated field effect transistors [19–21].

Here we employ electrolyte gating to control the electron concentration in the SEA with concurrent *in situ* optical probing by means of Raman spectroscopy. We note that a conceptually similar approach has been used to investigate near-surface electronic Raman scattering in graphene using electrolyte gating [22, 23] and in III–V semiconductors and silicon using metal-insulator-semiconductor structures [24, 25]. We provide definite proof of the surface origin of the controversial LO-like Raman scattering in InN. We find that the LO-like Raman feature is reversibly modulated with gate voltage and follows a universal behavior regardless of the bulk doping properties. The shifts of this peak with changes in the surface electron concentration are consistent with a Martin double resonance mechanism, in which larger phonon wavevectors become accessible under electron accumulation conditions due to band gap narrowing. We believe that the surface acts as mediator for the double resonance scattering process, contrary to what has been believed up to now. Moreover, the surface band gap narrowing should substantially influence the electron transport in SEA devices based on InN, and possibly, other small band gap semiconductors.

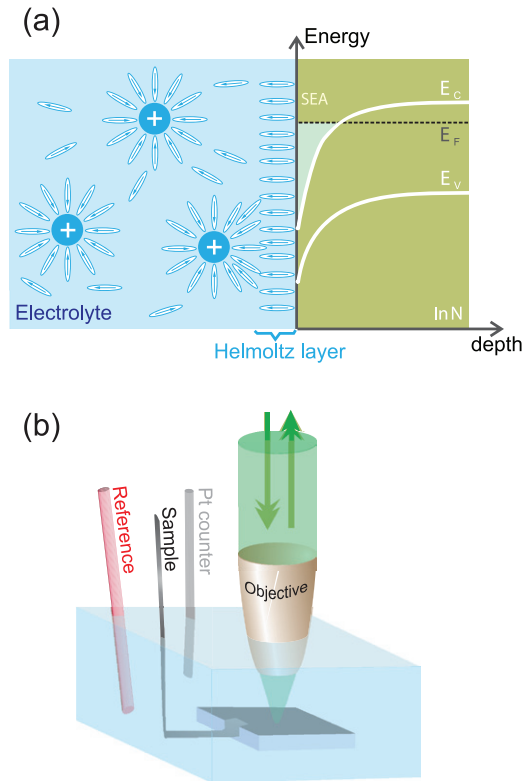


**Figure 1.** SEA and experimental configuration. In (a) the surface band bending of InN is depicted for a sample with a non degenerate  $n$ -type bulk doping behavior. The surface Fermi level is pinned above the conduction band minimum ( $E_c$ ), resulting in a SEA layer. The Helmholtz double layer which forms at the electrolyte/InN interface allows bias to be applied to the InN to either further accumulate or deplete the SEA. The optical measurement setup is shown in (b). Bias was applied to the InN with respect to the reference electrode using a standard 3-electrode configuration being controlled by a potentiostat. The microscope objective used to excite the InN surface and collect Raman scattered light was immersed in the electrolyte. It was chemically and electrically insulated from the electrolyte by a thin sheet of Teflon.

## 2. Experimental

InN thin films used in this study were grown by molecular beam epitaxy (MBE) on GaN templates. All films are  $c$ -axis oriented and have the wurtzite structure. Mg doping was used to produce  $p$ -type films [26, 27], while the  $n$ -type film was not intentionally doped. Details of the growth method and of the electrical characterization are reported elsewhere [27]. The samples were chosen to represent the range of  $n$ - and  $p$ -type InN available with MBE growth. The transport properties of the films used in this study are shown in table 1.

The optical and electrical measurement setup is shown in figure 1(b). Raman microprobe spectra were recorded at room temperature in the  $z(-, -)z$  scattering geometry. Laser excitation was provided either by a He–Ne (1.96 eV) or diode laser (2.33 eV) and the scattered light was collected by an optical microscope and was analyzed with a Jobin-Yvon LabRAM-HR spectrometer. A 0.5 M NaOH solution was used as the liquid electrolyte and a Biologic potentiostat was used to control the bias applied to the surfaces of the film. A water immersion objective ( $\times 64$ ) was used to focus the incident

**Table 1.** Structural and electrical transport properties of the InN films used in this study.

Sample	Film/buffer/template	$t$ (nm)	$n_e$ ( $10^{18} \text{ cm}^{-3}$ )	$\mu_e$ ( $\text{cm}^2 \text{ V}^{-1} \text{ s}^{-1}$ )	$S$ ( $\mu\text{V K}^{-1}$ )
N1	InN/GaN	500	2.7	1025	$-111(n)$
P1	InN:Mg/60 nm-InN/GaN	500	—	—	$-167(n)$
P2	InN:Mg/10 nm-InN/ GaN	1000	—	—	$+50(p)$
P3	InN:Mg/10 nm-InN/GaN	2000	—	—	$+270(p)$

*Note:* The thickness ( $t$ ) of the main InN layer excluding the buffer and the results of Hall ( $n_e$ ,  $\mu_e$ ) and Seebeck ( $S$ ) measurements are shown. Hall measurements for the 3 Mg-doped samples reflect electron transport in the accumulation layer only [26]; it is not possible to measure the hole concentration and mobility in the bulk of the film using this technique [27]. The positive value of the Seebeck coefficient for P2 and P3 confirms that the bulk of these films is  $p$ -type [26]. P1 is Mg doped but at a level below that of compensating donors, resulting in an overall negative Seebeck coefficient.

laser beam and collect the scattered light. It was chemically and electrically insulated from the electrolyte by a thin Teflon sheet [28]. The reference electrode was either Ag/AgCl or Hg/HgO and a platinum wire was used as the counter electrode. The sample potential was measured with respect to the reference electrode and is reported versus the normal hydrogen electrode (NHE). The surface of the InN thin films were HCl etched prior to the experiments in order to remove any surface oxides. Indium was used as ohmic contact to InN and was protected from the electrolyte by chemically resistant epoxy. The gate voltage was varied only in the regime in which there was negligible current flow between the InN and the electrolyte to prevent electrochemical reactions and/or etching of the film, both in the dark and under laser illumination.

We have shown previously that the insulating double layer which forms when a conformal liquid electrolyte is in contact with the surface of InN (figure 1(a)) allows bias potentials to be applied under conditions of minimal current flow. The electron concentration in the SEA in thin films can be increased, decreased to the bulk value (at the flat band potential), and even inverted to hole accumulation [29–31]. For the geometry employed here, more positive bias will deplete the surface while more negative bias will increase the electron accumulation. As we observed the largest effects in accumulation (see below), we will concentrate on changes caused by increasing the SEA with negative bias voltages.

### 3. Results

Capacitance–voltage ( $C$ – $V$ ) measurements were performed to determine the flat-band potential of the thin film samples, as shown in figure 2(a). In InN surface donors, ionized bulk donors/acceptors, and surface holes due to inversion at large positive biases all contribute to the observed capacitive space charge. As a result, the  $C$ – $V$  data do not follow a simple linear relationship when graphed in the Mott–Schottky ( $C^{-2}$  versus  $V$ ) form. Instead, quantitative analysis of  $C$ – $V$  data results requires solving the Poisson equation to determine the near surface electron concentration as a function of bias [16, 29]. Here, the 1D Poisson equation was solved by using the *nextnano*<sup>3</sup> software (copyright©2012, nextnano GmbH, Germany). The surface Fermi level pinning was taken into consideration by using a Schottky barrier of 650 mV at the InN surface. An ohmic back contact was used as the second boundary condition. The simulation allow the space charge density to be

calculated as a function of applied voltage. At 0V, the sheet electron density is between  $10^{13}$  and  $10^{14} \text{ cm}^{-2}$ , depending on doping, which is in agreement with experimental literature reports [13, 14, 30, 32]. Then, the capacitance was calculated from the derivative of the charge density as a function of voltage. A shift of 0.2 V was considered to account for the difference between the InN surface in air and water. The shift is taken from the difference between optical experiments in air and under water, described below. The  $C^{-2}$  versus  $V$  modeling results are shown as solid lines in figure 2(a). The good agreement of the model with the experimental data allows us to rule out any effects due to incorporation of ions into the near surface region. The doping densities used for the simulations are labeled in the figure. We find that the flat band potential for the  $n$ -type sample is  $\sim 0.35 \text{ V}$  versus NHE, while for  $p$ -type samples the flat band potentials are ca. 1 V versus NHE, with the difference corresponding approximately to the band gap of InN. The increase in slope of the  $C^{-2}$  versus  $V$  data with increasing positive bias reflects the change in contribution to the capacitance from the SEA to the space charge region in the bulk defined by the bulk doping as the surface condition is tuned from accumulation to depletion [16].

The solution to the Poisson equation also allows assessing the changes in band energy profiles as a function of voltage. Figure 2(b) shows the modulation given by the gate voltage to the InN surface band structure based on the assumed values in the capacitance-voltage simulations. Two doping conditions are plotted ( $N_D = 3 \times 10^{18} \text{ cm}^{-3}$  and  $N_A = 4 \times 10^{18} \text{ cm}^{-3}$ ). The near-surface band bending was calculated for InN under two different voltages ( $V = -1.2$  and  $+0.5 \text{ V}$  versus NHE), which represent a strong and moderate electron accumulation conditions. As can be observed, the band bending, and thus the electric field, strongly depends on the bulk doping concentration as well as gate voltage. Figure 2(c) shows the depth profile of the electron concentration for the same voltage inputs and bulk doping conditions. Although the depth profile of  $n_e$  strongly depends on bulk doping, the integrated sheet electron/hole accumulation (subtracting the bulk value) still remains rather similar for a large range of bulk concentrations and gate voltages (figure 2(d)). In essence, over the range of potentials ( $-1$  to  $+0.8 \text{ V}$  versus NHE) which will be employed in the *in situ* Raman experiments described below, the sheet carrier density in the SEA is modulated from  $<10^{11}$  to  $>10^{13} \text{ cm}^{-2}$ , according to our calculations.

Figure 3 shows the *in situ* Raman spectra as a function of bias from sample N1. In this backscattering geometry, the

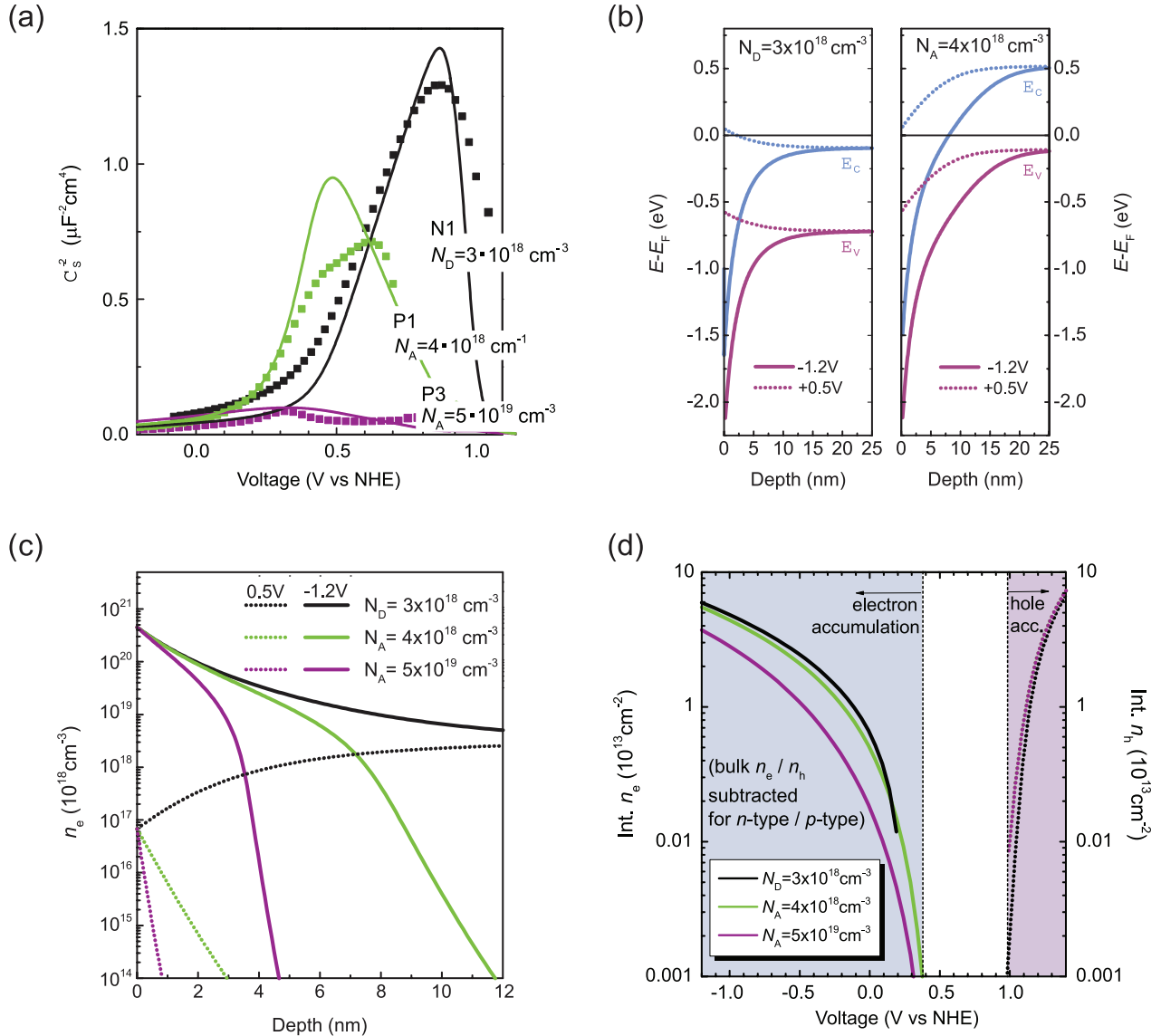


**Figure 2.** (a)  $1/C^2$  as a function of applied voltage to the semiconductor determined by electrochemical capacitance–voltage (ECV) measurements for differently doped InN samples used in this work along with three calculated curves for  $N_D = 3 \times 10^{18} cm^{-3}$ ,  $N_A = 4 \times 10^{18} cm^{-3}$  and  $N_A = 5 \times 10^{19} cm^{-3}$ . The measurements were performed at 1 kHz with 0.5 M NaOH solution as the electrolyte. Calculated lines were obtained by solving the Poisson equation. (b) Band bending under strong (solid lines) and moderate (dashed lines) accumulation conditions for two bulk doping values; degenerate  $n$ -type and non-degenerate  $p$ -type (c) Calculated electron concentrations for the strong and moderate accumulation conditions (d) Calculated integral electron density as a function of voltage for the same acceptor/donor bulk densities as in (a). The contribution from the bulk has been subtracted for clarity. Shaded blue (red) areas indicate the voltage region for which electrons (holes) are accumulated at the surface.

non-polar  $E_{2h}$  mode and the  $A_1(LO)$  mode are allowed by symmetry [12]. Spectra are normalized to the height of the  $E_{2h}$  phonon. As reported in many earlier works, the  $A_1(LO)$  peak is relatively more intense under red light excitation, indicating near resonance conditions, in spite of the large difference between the excitation energy (1.96 eV) and band gap of InN (0.69 eV) [33]. At a first glance, one can see that, regardless of excitation energy, the frequency of the LO-like scattering near  $590 cm^{-1}$  shifts to lower frequency as the electron accumulation is increased by applying a negative bias (gate changed from around +0.2 to  $-0.6 V$  versus NHE), while the  $E_{2h}$  peak is unchanged. This effect is completely reversible and the peak position returns to its original position when the potential is returned to above 0.2 V versus NHE. The

reversible shift of the LO-like feature with gate voltage was observed in all samples studied regardless of the bulk doping condition. Figure 4 shows exemplary spectra from all other samples which illustrate this point. Apart from the LO mode shift and broadening, which is common in all samples, there are more subtle changes in the spectra which occur under strong electron accumulation conditions. Close examination of the spectra in figures 3 and 4 show that a new peak ( $M1$ , at  $\sim 540 cm^{-1}$ ) and a shoulder on the LO phonon ( $M2$ ) appear under resonance conditions (633 nm wavelength). The possible origin of these modes will be discussed below.

In order to quantify changes in the LO peak as a function of voltage, we fit the spectra to Lorentzian lineshapes. In most cases, a weak disorder-activated longitudinal (DALO) band



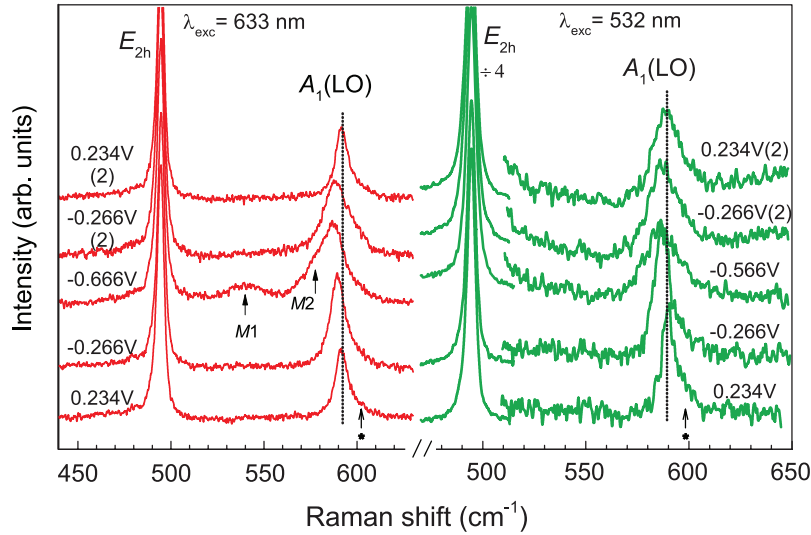


**Figure 3.** Raman spectra of *n*-InN (sample N1 in this manuscript) at 0V and at negative voltage (accumulation conditions) versus NHE with 633 nm (left) and 532 nm (right) excitation wavelengths. Spectra have been normalized to the  $E_{2h}$  intensity and are vertically shifted for clarity. The dotted vertical line indicates the position of the LO mode at 0.234V versus NHE. The voltage has been swept from 0.234 to  $-0.666$  V and back to 0.234 V versus NHE in order to show the reversibility of the effect (the order of the spectra is bottom to top). The DALO band is marked with an asterisk (see text).

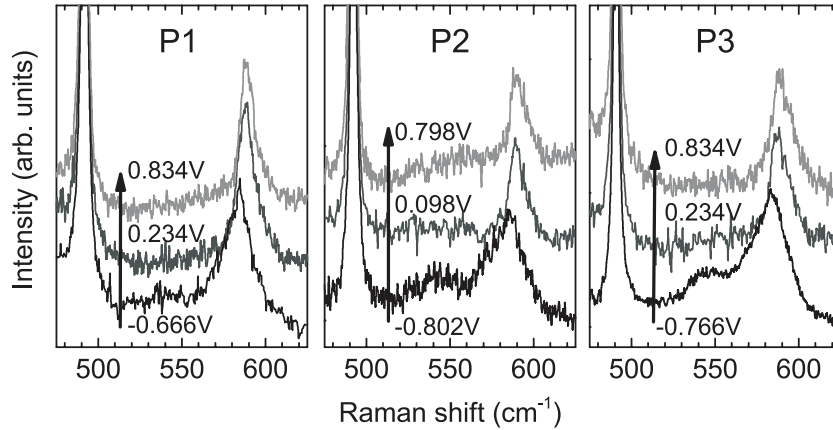


**Figure 4.** Raman spectra of Mg-doped InN (samples P1 to P3) at negative, 0V and positive voltage versus NHE. Spectra have been taken under red light excitation conditions. All spectra have been normalized to the  $E_{2h}$  intensity and are vertically shifted for clarity.

was included as a high frequency shoulder (marked with an asterisk in figure 3), and for the red-excited spectra, a third peak ( $M2$ ) has been taken into account for the deconvolution. We also corrected the peak frequencies of all features for strain caused by the heteroepitaxial growth using the difference in  $E_{2h}$  frequency with respect to the reported unstrained value of  $491.5 \text{ cm}^{-1}$  in [2 and 8] and using the values for the relationship between the frequency shift and strain ( $\Delta\omega/\Delta\sigma_a$ ) for the  $E_{2h}$  and  $A_1(\text{LO})$  modes of  $-9 \text{ cm}^{-1} \text{ GPa}^{-1}$  and  $-8.4 \text{ cm}^{-1} \text{ GPa}^{-1}$ , respectively [34], where  $\sigma_a$  is the biaxial stress and  $\Delta\omega$  is the strain-induced shift. Figure 5(a) summarizes the shift of the LO phonon as a function of bias for all thin films samples. The FWHM of the main LO peak is shown as a function of bias in figure 5(b). Figure 5 shows that the changes in the LO phonon scattering produced by electrolyte gating are large: the peak frequency red shifts by up to  $\sim 6 \text{ cm}^{-1}$  and its FWHM increases by nearly a factor of two under accumulation conditions. It is also clear that the *n*-type and the three Mg-doped samples show a universal behavior, within our experimental

resolution, in terms of the accumulation-induced red-shift and broadening of the LO phonon feature for both laser excitation wavelengths.

#### 4. Discussion

We begin with a discussion of the LO phonon scattering and how it is affected by gate voltage. As shown in figures 2(b) and (c), electrolyte gating produces changes in the electron concentration in only the top ca. 10 nm of the InN films. Thus, the observation that the  $A_1(\text{LO})$  Raman peak shifts controllably and reversibly with the applied potential clearly demonstrates the surface origin of this feature. As seen in figure 5(a), the frequency trend of the LO mode is the same for all four of the InN samples studied in this work and for both laser excitations: the more negative the voltage, i.e. the more electron accumulation, the lower the LO frequency.

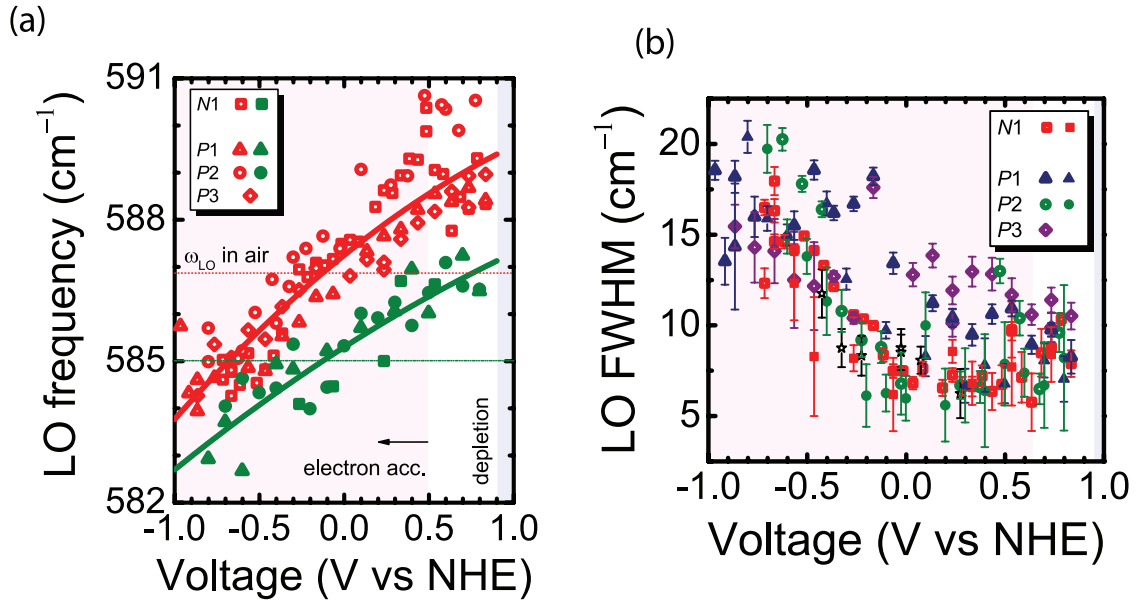


**Figure 5.** (a) Frequency of the LO Raman peak (strain corrected) for the differently doped InN samples as a function of voltage. Empty (filled) data points were obtained by using the 632.8 nm (532 nm) excitation line. The red dotted (green dashed) line corresponds to the frequency of the LO mode of InN in air probed by 632.8 nm (532 nm) laser line. The red (blue) shadowed area indicates the voltage range for which electrons (holes) are being accumulated at the surface (b) Voltage dependence of the LO peak FWHM.

The dotted red and green horizontal lines in figure 5(a) indicate the frequency position of the  $A_1(\text{LO})$  peak in air. As mentioned above, the frequency in air is obtained again under electrolyte controlled conditions at  $-0.2\text{V}$  versus NHE, indicating a slight depletion effect created by the water electrolyte immersion. The  $A_1(\text{LO})$  frequency in air is about  $2\text{cm}^{-1}$  larger for red excitation compared to green in agreement with the study of Davydov *et al* [8]. In that study, it was proposed that Martin's double resonance is responsible for the observation of  $A_1(\text{LO})$  with large values of the phonon wavevector  $q$  [8]. In their work, they observe a red-shift of the LO phonon with increasing the excitation energy, consistent with the prediction that the phonon wavevector ( $q_{\text{ph}}$ ) can be twice that of the photoexcited electron-hole ( $k_{\text{eh}}$ ), as shown schematically in figure 6. Thus, an increase in the above bandgap excitation energy will allow electrons to be promoted to the conduction band at larger  $k_{\text{eh}}$ , and in turn are able to scatter LO phonons of larger  $q_{\text{ph}}$ . Our observation of a larger  $\omega_0$  for red versus green excitation is clearly consistent with this mechanism.

The present work clearly demonstrates the surface nature of the LO feature, given by the ability to tune its frequency through modulating the electron concentration at the surface. Kranert *et al* have recently proposed a model in which surface defects can lead to the wavevector non-conservation required for large  $q_{\text{ph}}$  to be observed in wurtzite material [12]. The fact that the surface can act as a planar defect, allowing the 1LO resonant mode to be scattered, can explain both the presence of Martin's double resonance in high quality InN and our findings. Regarding the large frequency shift produced by tuning the gate voltage, we are evidently probing  $A_1(\text{LO})$  with different  $q_z$  across the Brillouin zone (BZ). Calculations of the phonon dispersion in wurtzite InN of the  $A_1(\text{LO})$  dispersion from the  $\Gamma$  point to the  $A$  point predict a red-shift of  $8\text{--}10\text{cm}^{-1}$  across the width of the zone

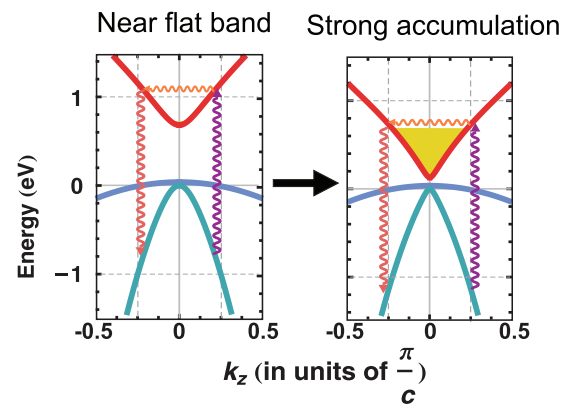


**Figure 6.** Schematic diagram of the proposed scattering mechanism as a function of band gap renormalization. The dispersion is given for wavevectors along the [0001] direction (i.e. along the  $\Gamma$ -A line). The excitation energy is 1.96 eV. The surface allows elastic scattering of the exciton to give rise to long-wavevector phonons with  $q_{\text{ph}} = 2k_z$  (horizontal arrows). Only optical transitions from the split-off to the conduction band are shown (see text).

[8, 35]. Considering both laser excitations, the data shown in figure 5(a), in which the electrolyte gating tunes the  $A_1(\text{LO})$  frequency from  $\sim 590\text{cm}^{-1}$  (red excitation, depletion) to  $\sim 583\text{cm}^{-1}$  (green excitation), suggests that a wide range of  $q$  is being accessed. We will explain this effect by a combination of a Martin double resonance, the surface origin of the momentum non-conservation, and an SEA-induced change in the surface band structure.

It is known that high electron concentrations reduce the band gap, both in the bulk [36] and in 2D structures [37, 38]. Thus, it would be expected that the band gap near the surface of InN would be reduced as compared to the bulk as a result of the electron accumulation. Indeed, this effect has been quantified experimentally for InN by angle resolved photoemission

by King *et al* [39] Remarkably, for InN samples in vacuum, the surface band gap was reduced by 450 meV compared to the bulk value (690 meV). For our work, we expect a similar reduction in the surface band gap in air and an even larger reduction by increasing the SEA through gating.

It is possible to estimate the range of  $q$  accessible by the laser excitation energies we used and with the magnitudes of  $n_{\text{surface}}$  available by electrolyte gating shown in figures 2(c)–(d). It is known that the band gap shrinkage scales with  $(n_{\text{surface}})^{1/3}$ , as has been experimentally predicted and observed in many systems [37, 38, 40]. In the work by King *et al* the 2D carrier density was  $\sim 1.6 \times 10^{13} \text{ cm}^{-2}$  before renormalization. This corresponds to an electron concentration at the surface of  $\sim 2 \times 10^{20} \text{ cm}^{-3}$ , according to our calculations as described above. Using the reported band gap reduction of 450 meV, we obtain

$$\Delta E_g \approx -7.69 \times 10^{-5} \text{ meV cm } (n_{\text{surface}})^{1/3}. \quad (1)$$

Referring to figures 2(b)–(d) and to equation (1), we estimate a bandgap reduction of  $\sim 550$  meV for the largest negative potential used in this study ( $V = -1$  V versus NHE). Similarly, the full InN bandgap ( $\Delta E_g = 0$ ) at the surface is expected for a voltage of  $+0.6$  V versus NHE and above.

We used  $8 \times 8$   $k$ - $p$  theory to apportion the band gap reduction between the conduction and valence bands [41, 42]. For the scattering results discussed here, with the surface acting as a planar defect allowing the transfer of momentum from the photoexcited charge to the lattice, along the  $[0001]$  direction. In this direction, the light holes and heavy holes in InN have a similar effective mass, about  $1.56 m_e$  [43]. Lighter holes are found at the split-off band with an effective mass of  $0.12 m_e$ . In the  $8 \times 8$   $k$ - $p$  analysis, which is performed for  $k_x = k_y = 0$  and  $k = k_z$ , we include the crystal field splitting, spin orbit interaction and band gap reduction. The band dispersions is found by diagonalizing the following Hamiltonian:

$$H_{8 \times 8} = \begin{pmatrix} Ec + \frac{\hbar^2 k^2}{2 m_e} & 0 & 0 & kP & 0 & 0 & 0 & 0 \\ 0 & F + \frac{\Delta_{\text{SO}}}{3} & 0 & 0 & 0 & 0 & 0 & 0 \\ 0 & 0 & F - \frac{\Delta_{\text{SO}}}{3} & 0 & 0 & 0 & 0 & \frac{\sqrt{2}}{3} \Delta_{\text{SO}} \\ kP & 0 & 0 & \lambda & 0 & 0 & \frac{\sqrt{2}}{3} \Delta_{\text{SO}} & 0 \\ 0 & 0 & 0 & 0 & Ec + \frac{\hbar^2 k^2}{2 m_e} & 0 & 0 & kP \\ 0 & 0 & 0 & 0 & 0 & F + \frac{\Delta_{\text{SO}}}{3} & 0 & 0 \\ 0 & 0 & 0 & \frac{\sqrt{2}}{3} \Delta_{\text{SO}} & 0 & 0 & F - \frac{\Delta_{\text{SO}}}{3} & 0 \\ 0 & 0 & \frac{\sqrt{2}}{3} \Delta_{\text{SO}} & 0 & kP & 0 & 0 & \lambda \end{pmatrix}, \quad (2)$$

where

$$E_C = E_g + \Delta_{\text{CF}} + \frac{1}{3} \Delta_{\text{SO}}, \quad (3a)$$

$$F = \Delta_{\text{CF}} + \lambda + \theta, \quad (3b)$$

$$\lambda(k) = \frac{\hbar^2 k^2}{m_0} A_1, \text{ and} \quad (3c)$$

$$\theta(k) = \frac{\hbar^2 k^2}{m_0} A_3. \quad (3d)$$

$P$  is the Kane parameter ( $0.757 \text{ eV nm}$ ),  $\Delta_{\text{CF}} = 40$  meV,  $\Delta_{\text{SO}} = 5$  meV, and  $E_g = 0.69 \text{ eV} + \Delta E_g$  where  $\Delta E_g$  is calculated from equation (1).  $A_i$  are valence band parameters defined as follows:

$$m_{hh}^* = -m_0(A_1 + A_3)^{-1} \text{ and} \quad (4a)$$

$$m_{ch}^* = -m_0 \left( A_1 + \frac{E_{ch}^0}{E_{ch}^0 - E_{lh}^0} A_3 \right)^{-1}, \text{ where} \quad (4b)$$

$$E_{ch}^0 = \frac{3\Delta_{\text{CF}} - \Delta_{\text{SO}}}{6} - \frac{1}{2} \sqrt{\Delta_{\text{CF}}^2 + \Delta_{\text{SO}}^2 - \frac{2}{3} \Delta_{\text{SO}} \Delta_{\text{CF}}} \text{ and} \quad (4c)$$

$$E_{lh}^0 = \frac{3\Delta_{\text{CF}} - \Delta_{\text{SO}}}{6} + \frac{1}{2} \sqrt{\Delta_{\text{CF}}^2 + \Delta_{\text{SO}}^2 - \frac{2}{3} \Delta_{\text{SO}} \Delta_{\text{CF}}}. \quad (4d)$$

To obtain  $m_{hh}^* = 1.56 m_e$ , and  $m_{so}^* = 0.12 m_e$  at the valence band maximum,  $A_1 = -8.36$  and  $A_3 = 7.72$ . An approximation for small wavevectors was used by Davydov *et al* where a 2-band interaction between the lightest holes and the conduction band was considered, with a non-interacting heavy hole band [8].

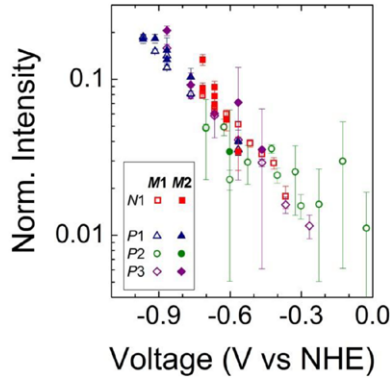


**Figure 7.** Normalized intensity of features *M1* and *M2* (see figure 3(a)) as a function of bias. Normalization is performed with respect to the  $E_{2h}$  mode. The y-axis is in logarithmic scale.

Figure 6 shows the evolution of the band structure and electron dispersion perpendicular to the surface as the condition is changed from flat-band (no accumulation) to strongly accumulated (from 0 to 550 meV in band gap reduction, equation (2)). It is clear that not only the band gap energy decreases with electron accumulation, but also the band edges become sharper resembling those of graphene. In each case, a Martin's double resonance scattering is also shown schematically, where the surface is responsible for the wave-vector non-conservation along the  $z$ -direction [12].

By considering the band bending simulations shown in figure 2, along with equations (1) and (2), we estimate that the phonon wavevector  $q_{ph}$  range that is accessed by electrolyte gating ranges from 0.452 to 0.52 (in units of  $\pi/c_0$ ) and from 0.538 to 0.606 (in units of  $\pi/c_0$ ), for the red and green light excitations, respectively. This means, that by applying a gate voltage to our InN films, phonons within the second half of the BZ along the  $\Gamma$ - $A$  direction are sampled, where the more negative voltages produce scattering from phonons the closer to the zone edge. These values were obtained by considering only the split-off band. For heavy holes, the  $q_{ph}$  resides outside the BZ. Moreover, as we observe a smooth trend of the experimental phonon frequency with voltage, we do not believe that resonances involving other bands make a large contribution to the scattering.

In order to correlate these findings with the experimental results, we use the LO phonon dispersion to find the frequency range accessed by surface gating. By taking the dispersion given in [8], we find that for going from flat band to strong surface accumulation, the LO phonon should shift from 585.7 to 583.5  $\text{cm}^{-1}$  for the red light excitation. For green light excitation, the predicted frequency range is from 583.0 to 580.6  $\text{cm}^{-1}$ . In both cases, the experimental shift is in the same direction as the model, but the observed shift is somewhat larger (4–5.5 versus 2–2.4  $\text{cm}^{-1}$ , for red and green excitations respectively). We note, however, that there are uncertainties in both the effective mass parameters and phonon dispersion for InN, which may explain some of the discrepancy. It is also possible that the large electric field produced by the strong surface band bending plays a role.

Now, we turn to the origin of the broadening under strong electron accumulation, figure 5(b). We note that the maximum line widths observed, ca. 20  $\text{cm}^{-1}$ , are larger than the predicted

maximum dispersion of the  $A_1(\text{LO})$  phonon from zone center to edge. We believe that the phonon lifetime is decreased under strong electron accumulation conditions, which will cause additional Raman line broadening.

Finally, we want to address the observation of the two peaks (labeled *M1* and *M2* in figure 3) that are observed for negatively gated InN. The feature *M1* is the most clear and appears at a frequency of around 540  $\text{cm}^{-1}$ . We note that the frequency is very close to that of the forbidden  $B_{1h}$  silent mode which has been observed experimentally in the near surface region by second harmonic generation spectroscopy [44]. *M2* is a shoulder on the LO feature at about 585  $\text{cm}^{-1}$ . The observation of Raman peaks around the frequencies of *M1* and *M2* have been reported in other studies [5, 45–49]. While some attribute it to the  $B_1$  silent mode arising from sample imperfections, others have assigned them to surface optical (SO) modes with  $A_1$  and  $E_1$  symmetries. Interestingly, Schäfer-Nolte *et al* suspected that these peaks appearing in highly doped samples could be related to electron transitions at localized states [46]. In our work, we see that both features are clearly enhanced by long wavelength excitation and the presence of large electron densities at the surface, which follows the theory of electron-related transitions. Figure 7 shows the intensity trend of these two features as a function of applied voltage. It is clear from the identical exponential increase in intensity of *M1* and *M2*, regardless of sample nature, that there is a direct link between carrier density and/or band structure at the surface and these Raman features.

## 5. Conclusions

*In situ* micro-Raman measurements were used to probe directly the interaction between the SEA layer and the Raman-active phonons. We find that the intensity and frequency of the forbidden LO Raman feature is reversibly changed by the external potential, showing its surface origin. This is the first experimental evidence of the relation between the LO feature in InN and free electron accumulation at its surface. Martin's double resonance mechanism is responsible for long-wavelength LO scattering at the InN surface. By changing the band bending at the surface, both carrier density and band structure are modulated, which in turn changes range of LO phonon wavevectors which contribute to the scattering.

The changes in the surface band structure produced by controlling the SEA are significant. Under condition of maximum accumulation, the surface band gap is predicted to be reduced from its bulk value of 0.65 eV by over 0.5 eV and our  $8 \times 8$   $k$ - $p$  analysis predicts that the band edges should become very sharp, resembling those of graphene. This would be expected to have a large influence on the electron transport in the SEA. Under condition of electron depletion, the surface band gap should be similar to the bulk value.

## Acknowledgments

This work was supported by Director, Office of Science, Office of Basic Energy Sciences, Materials Sciences and



Engineering Division, of the U.S. Department of Energy under Contract No. DE-AC02-05CH11231. EAL acknowledges the support from the Marie Curie Actions. TB acknowledges the support by the EU under the Grant Agreement No. PITN-GA-2008-213238, Initial training network RAINBOW of the 7 RTD Framework. We thank Alex Bell, Jason Yeo Boon Siang and Mary Louie for the use of their Raman microprobe instruments. We also thank Jordi Ibáñez Insa for fruitful discussions.

## References

- [1] Cardona M and Guntherodt G 1984 *Light Scattering in Solids IV* (Berlin: Springer)
- [2] Davydov V Y, Emtsev V V, Goncharuk I N, Smirnov A N, Petrikov V D, Mamutin V V, Vekshin V A, Ivanov S V, Smirnov M B and Inushima T 1999 *Appl. Phys. Lett.* **75** 3297
- [3] Ager J W, Walukiewicz W, Shan W, Yu K M, Li S X, Haller E E, Lu H and Schaff W J 2005 *Phys. Rev. B* **72** 155204
- [4] Kasic A, Schubert M, Saito Y, Nanishi Y and Wagner G 2002 *Phys. Rev. B* **65** 115206
- [5] Thakur J S, Haddad D, Naik V M, Naik R, Auner G W, Lu H and Schaff W J 2005 *Phys. Rev. B* **71** 115203
- [6] Demangeot F, Pinquier C, Frandon J, Gaio M, Briot O, Maleyre B, Ruffenach S and Gil B 2005 *Phys. Rev. B* **71** 104305
- [7] Cuscó R, Ibáñez J, Alarcón-Lladó E, Artús L, Yamaguchi T and Nanishi Y 2009 *Phys. Rev. B* **80** 155204
- [8] Davydov V Y, Klochikhin A A, Smirnov A N, Strashkova I Y, Krylov A S, Lu H, Schaff W J, Lee H-M, Hong Y-L and Gwo S 2009 *Phys. Rev. B* **80** 81204
- [9] Martin R 1974 *Phys. Rev. B* **10** 2620
- [10] Domènech-Amador N, Cuscó R, Calarco R, Yamaguchi T, Nanishi Y and Artús L 2012 *Phys. Status Solidi: Rapid Res. Lett.* **6** 160
- [11] Cho Y, Ramsteiner M and Brandt O 2013 *Appl. Phys. Lett.* **102** 72101
- [12] Kranert C, Schmidt-Grund R and Grundmann M 2013 *New J. Phys.* **15** 113048
- [13] Colakerol L et al 2006 *Phys. Rev. Lett.* **97** 237601
- [14] Mahboob I, Veal T D, McConville C F, Lu H and Schaff W J 2004 *Phys. Rev. Lett.* **92** 36804
- [15] King P D C et al 2007 *Appl. Phys. Lett.* **91** 92101
- [16] Yim J W L, Jones R E, Yu K M, Ager J W, Walukiewicz W, Schaff W J and Wu J 2007 *Phys. Rev. B* **76** 41303
- [17] Lu H, Schaff W J and Eastman L F 2004 *J. Appl. Phys.* **96** 3577
- [18] Lu Y-S, Huang C-C, Yeh J A, Chen C-F and Gwo S 2007 *Appl. Phys. Lett.* **91** 202109
- [19] Lin Y-S, Koa S-H, Chan C-Y, Hsu S S H, Lee H-M and Gwo S 2007 *Appl. Phys. Lett.* **90** 142111
- [20] Lu Y-S, Chang Y-H, Hong Y-L, Lee H-M, Gwo S and Yeh J A 2009 *Appl. Phys. Lett.* **95** 102104
- [21] Chen Z Y, Yuan H T, Wang X Q, Ma N, Zhang Y W, Shimotani H, Qin Z X, Shen B and Iwasa Y 2013 *Appl. Phys. Lett.* **103** 253508
- [22] Cronin S B, Barnett R, Tinkham M, Chou S G, Rabin O, Dresselhaus M S, Swan A K, Ünlü M S and Goldberg B B 2004 *Appl. Phys. Lett.* **84** 2052
- [23] Das A et al 2008 *Nat. Nanotechnol.* **3** 210
- [24] Abstreiter G, Claessen U and Tränkle G 1982 *Solid State Commun.* **44** 673
- [25] Abstreiter G, Huber R, Tränkle G and Vinter B 1983 *Solid State Commun.* **47** 651
- [26] Miller N et al 2010 *J. Appl. Phys.* **107** 113712
- [27] Wang K et al 2011 *Appl. Phys. Lett.* **98** 42104
- [28] Yeo B S, Klaus S L, Ross P N, Mathies R A and Bell A T 2010 *Chem. Phys. Chem.* **11** 1854
- [29] Ager J W, Miller N, Jones R E, Yu K M, Wu J, Schaff W J and Walukiewicz W 2008 *Phys. Status Solidi* **245** 873
- [30] Brown G F, Ager J W III, Walukiewicz W, Schaff W J and Wu J 2008 *Appl. Phys. Lett.* **93** 262105
- [31] Khanal D R, Walukiewicz W, Grandal J, Calleja E and Wu J 2009 *Appl. Phys. Lett.* **95** 173114
- [32] Lu H, Schaff W J, Eastman L F and Stutz C E 2003 *Appl. Phys. Lett.* **82** 1736
- [33] Inushima T, Higashiwaki M and Matsui T 2003 *Phys. Rev. B* **68** 235204
- [34] Wang X, Che S-B, Ishitani Y and Yoshikawa A 2006 *Appl. Phys. Lett.* **89** 171907
- [35] Bungaro C, Rapcewicz K and Bernholc J 2000 *Phys. Rev. B* **61** 6720
- [36] Berggren K and Sernelius B 1981 *Phys. Rev. B* **24** 1971
- [37] Das Sarma S, Jalabert R and Yang S-R E 1989 *Phys. Rev. B* **39** 5516
- [38] Jalabert R and Das Sarma S 1989 *Phys. Rev. B* **40** 9723
- [39] King P D C, Veal T D, McConville C F, Zúñiga-Pérez J, Muñoz-Sanjósé V, Hopkinson M, Rienks E D L, Jensen M F and Hofmann P 2010 *Phys. Rev. Lett.* **104** 256803
- [40] Tränkle G, Leier H, Forchel A, Haug H, Ell C and Weimann G 1987 *Phys. Rev. Lett.* **58** 419
- [41] Kane E O 1957 *J. Phys. Chem. Solids* **1** 249
- [42] Chuang S and Chang C 1996 *Phys. Rev. B* **54** 2491
- [43] Wu J 2009 *J. Appl. Phys.* **106** 11101
- [44] Chang Y-M, Chu H W, Shen C-H and Gwo S 2007 *Appl. Phys. Lett.* **90** 72110
- [45] Pomeroy J W, Kuball M, Swartz C H, Myers T H, Lu H and Schaff W J 2007 *Phys. Rev. B* **75** 35205
- [46] Schäfer-Nolte E O, Stoica T, Gotschke T, Limbach F A, Sutter E, Sutter P, Grützmacher D and Calarco R 2010 *Nanotechnology* **21** 315702
- [47] Jeganathan K, Purushothaman V, Debnath R K, Calarco R and Luth H 2010 *Appl. Phys. Lett.* **97** 93104
- [48] Sahoo S, Hu M S, Hsu C W, Wu C T, Chen K H, Chen L C, Arora A K and Dhara S 2008 *Appl. Phys. Lett.* **93** 233116
- [49] Zhu J H, Ning J Q, Zheng C C, Xu S J, Zhang S M and Yang H 2011 *Appl. Phys. Lett.* **99** 113115